Magnetic microposts as an approach to apply forces to living cells

Nathan J. Sniadecki*, Alexandre Anguelouch†, Michael T. Yang*, Corinne M. Lamb†, Zhijun Liu*, Stuart B. Kirschner†, Yaohua Liu†, Daniel H. Reich†, and Christopher S. Chen*‡

*Department of Bioengineering, University of Pennsylvania, 510 Skirkanich Hall, 210 South 33rd Street, Philadelphia, PA 19104; and †Department of Physics and Astronomy, The Johns Hopkins University, 3400 North Charles Street, Baltimore, MD 21218

Edited by David Mooney, Harvard University, Cambridge, MA, and accepted by the Editorial Board July 14, 2007 (received for review January 3, 2007)

Cells respond to mechanical forces whether applied externally or generated internally via the cytoskeleton. To study the cellular response to forces separately, we applied external forces to cells via microfabricated magnetic posts containing cobalt nanowires interspersed among an array of elastomeric posts, which acted as independent sensors to cellular traction forces. A magnetic field induced torque in the nanowires, which deflected the magnetic posts and imparted force to individual adhesions of cells attached to the array. Using this system, we examined the cellular reaction to applied forces and found that applying a step force led to an increase in local focal adhesion size at the site of application but not at nearby nonmagnetic posts. Focal adhesion recruitment was enhanced further when cells were subjected to multiple force actuations within the same time interval. Recording the traction forces in response to such force stimulation revealed two responses: a sudden loss in contractility that occurred within the first minute of stimulation or a gradual decay in contractility over several minutes. For both types of responses, the subcellular distribution of loss in traction forces was not confined to locations near the actuated micropost, nor uniformly across the whole cell, but instead occurred at discrete locations along the cell periphery. Together, these data reveal an important dynamic biological relationship between external and internal forces and demonstrate the utility of this microfabricated system to explore this interaction.

focal adhesions | magnetic nanowires | mechanotransduction | microfabrication | traction forces

Mechanical forces contribute to many cellular functions, including changes in gene expression, proliferation, and differentiation (1). Applying shear or tensile stresses to cells in culture, for example, can induce changes in adhesion regulation, intracellular signaling, and cell function (2–4). In addition to external forces, cells generate internal, cytoskeletally mediated traction forces that also play a vital role in cellular regulation (5, 6). The similarities in cellular responses to externally applied and internally generated forces have led to the suggestion that both types of forces may use shared mechanotransduction pathways to convert mechanical stimuli into biochemical signals (7, 8).

Although several structures within cells are involved in mechanotransduction, focal adhesions (FAs) appear to play a central role in sensing both external and internal forces. FAs arise from the clustering of integrins upon attachment to the extracellular matrix, which both recruits scaffolding proteins that mechanically connect FAs to the actin cytoskeleton and engages numerous proteins involved in adhesion and growth factor signaling. Importantly, maturation and signaling of FAs appear to depend on mechanical factors. The amount of FA protein accumulation in each adhesion correlates with local traction force (9, 10), and inhibiting cytoskeletal tension disassembles existing FAs and abrogates new FA assembly (11, 12). Moreover, FA growth also can be induced through application of external force (4, 13, 14). Similarly, numerous signaling pathways associated with FAs can be regulated by externally applied forces (15, 16), further suggesting a general role for FAs in mechanotransduction.

Although externally applied and internally generated forces may act independently on cells, it is quite likely that they are coupled. External forces can cause adhesion reinforcement (17–19) and stress fiber formation (20) to strengthen traction forces and appear to initiate specific signaling pathways that may provide feedback to regulate myosin activity (3, 21). Thus, it remains unclear whether external forces act directly or also depend on mechanically induced changes in traction forces to exert their cellular effects. Techniques to measure traction forces or to apply forces to cells are available (1, 22–24), but not to do both simultaneously.

Here, we present a strategy to apply external forces and monitor changes in traction forces by using microfabricated arrays of magnetic and nonmagnetic silicone elastomeric posts. A few microposts interspersed among nonmagnetic sensor posts contain embedded magnetic nanowires. In a magnetic field, posts with nanowires apply an external force to cells cultured on the tops of the posts. Nonmagnetic posts deflect in response to, and therefore report, traction forces of the cells. Using this system, we observed local FA growth at magnetically actuated posts only and not at nonmagnetic sensor posts. We also recorded a loss in traction forces upon local force application that was widespread, but not uniform, across the cells. These data suggest that cells actively adjust their internal tension to mechanical forces arising in their microenvironment and highlight the need to characterize mechanical feedback in cells.

Results

Fabrication of Magnetic and Nonmagnetic Post Arrays. To construct the magnetic and nonmagnetic post arrays, we incorporated magnetic Co nanowires with diameter 350 nm and length L_W = 5–7 μm into our previously developed microfabricated arrays of poly(dimethylsiloxane) (PDMS) microposts with post diameter D = 3 μm, length L = 10 μm, and center-to-center spacing of 9 μm (10). Nonmagnetic sensor posts behave like simple springs with bending deflections δ that are linearly proportional to the traction force F exerted on them by adherent cells (25). Embedding magnetic nanowires into a subset of posts allowed us to magnetically actuate those posts. A horizontal magnetic field $\vec{B}$ produces a torque $\vec{\tau} = \vec{\mu} \times \vec{B}$ on the magnetic moment $\vec{\mu}$ of a nanowire. This torque imparts a bending stress to the micropost, which is transmitted to an attached cell as an external force F_{Mag} (Fig. 1*A*). With a uniform field applied across the array, external

Author contributions: N.J.S., D.H.R., and C.S.C. designed research; N.J.S., A.A., M.T.Y., C.M.L., Z.L., S.B.K., Y.L., and D.H.R. performed research; and N.J.S., D.H.R., and C.S.C. wrote the paper.

The authors declare no conflict of interest.

This article is a PNAS Direct Submission. D.M. is a guest editor invited by the Editorial Board.

Abbreviations: FA, focal adhesion; PDMS, poly(dimethylsiloxane).

‡To whom correspondence should be addressed. E-mail: chrischen@seas.upenn.edu.

This article contains supporting information online at www.pnas.org/cgi/content/full/0611613104/DC1.

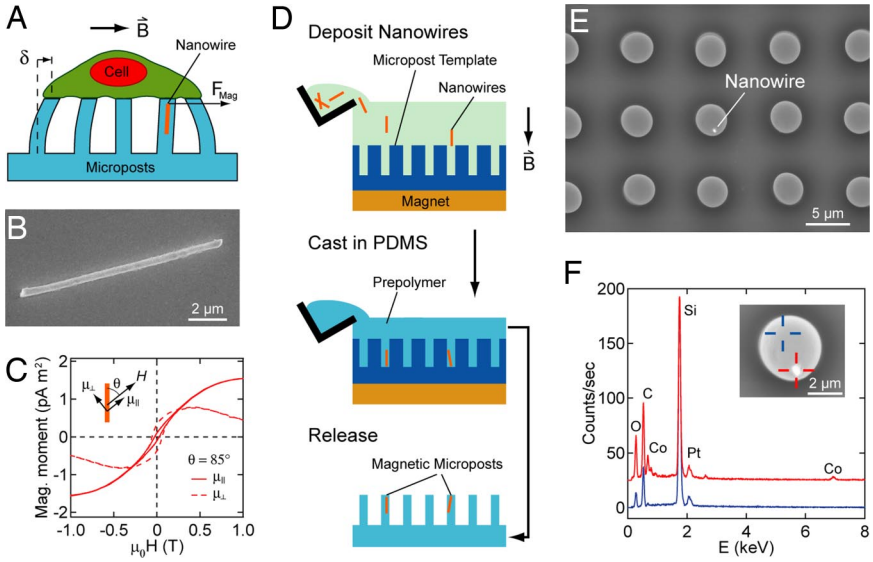

Fig. 1. Microfabricated arrays of magnetic and nonmagnetic posts for applying external forces and measuring traction force response. (*A*) External force F_{Mag} is applied to the adherent cell through magnetic posts embedded with Co nanowires that bend under the influence of a magnetic field, $\vec{B}$ (not drawn to scale). Nonmagnetic posts report local traction forces through post deflections δ. (*B*) SEM micrograph of a Co nanowire. (*C*) Magnetic moment components per wire $\mu_{|}$ and $\mu_{\perp}$ for 15-μm-long Co nanowires versus applied magnetic field $\mu_0 H$ as measured by vibrating sample magnetometer for $\vec{H}$ oriented at $\theta = 85°$ to the nanowires (*Inset*). $\vec{\mu}$ scales simply with nanowire length (32), so these results are representative of the wires used in the magnetic posts. (*D*) Process flow diagram for embedding nanowires into the micropost. (*E*) SEM backscattering micrograph showing a nanowire in the micropost array. (*F*) Energy-dispersive x-ray microanalysis measurements for bright material (red curve; *Inset*, red cross-hairs) within the magnetic posts observed under backscattering SEM (*Inset*). Areas nearby do not contain Co (blue curve; *Inset*, blue cross-hairs). The red curve is offset by 25 counts per sec to clarify between curves.

forces can be applied to many cells in parallel while measuring their mechanical response. An example of a Co nanowire is shown in Fig. 1*B*. Fig. 1*C* shows the vector components $\mu_{|}$ and $\mu_{\perp}$ of the magnetic moment per wire, measured for a collection of aligned nanowires with $\vec{B}$ oriented at 85° to the nanowires' long axis (Fig. 1*C Inset*). The large $\mu_{\perp}$ arises from magnetic shape anisotropy that favors alignment of $\vec{\mu}$ along a wire's long axis (26). To make the magnetic and nonmagnetic post arrays, nanowires were aligned with a vertical magnetic field, precipitated from suspension into casting templates at densities of one wire per 200 posts, and then encapsulated when the posts were formed by replica-molding (Fig. 1*D*). We confirmed the presence of the nanowires by SEM backscattering, in which nanowires appear as bright spots (Fig. 1*E*). Energy-dispersive x-ray microanalysis spectra verified that the characteristic Co x-ray peaks at 0.78 keV (Lα) and 6.93 keV (Kα) were observed only at the locations of the nanowires (Fig. 1*F*).

Characterization of Magnetic Post Actuation. To measure the actuation of magnetic posts from the induced torque $\vec{\tau}$, we applied a uniform horizontal magnetic field $\vec{B}$ by using electromagnets mounted on a microscope stage (Fig. 2*A*). The magnetic posts were identified under phase-contrast microscopy (Fig. 2*B*). Applying a field $\vec{B} = 0.31$ T to the array gave displacements δ_M to the magnetic posts in the range of 500 nm to 1 μm (Fig. 2*C*). To characterize the displacement versus field relationship, $\vec{B}$ was cycled between -0.31 T and 0.31 T while imaging the magnetic posts and their nonmagnetic neighbors [supporting information (SI) Movie 1]. The displacements of the tops of the posts were calculated from their centroid positions in each frame to provide δ_M versus B curves (Fig. 2*D*).

For a given magnetic post, δ_M is always in the same direction, independent of the sign of $\vec{B}$, because the nanowires' magnetic moment changes sign with $\vec{B}$ (Fig. 1*C*), and therefore $\vec{\tau}$ does not change sign. SEM observations showed that nanowires typically are tipped at a small angle up to 15° from vertical inside the posts (data not shown). As a result, $\vec{B}$ is not exactly perpendicular to the nanowires' long axis, which leads to a large $\mu_{\perp}$ (26), as seen in Fig. 1*C*. Noting that the scalar value of the torque is $\tau = \mu_{\perp} B$, and that $\delta_M \propto \tau$ for a cantilever beam such as the microposts (27), the measured $\mu_{\perp}$ (Fig. 1*C*) accounts for the unidirectional, quasi-quadratic, and hysteretic behavior observed in δ_M versus B (Fig. 2*D*).

The magnitude of δ_M indicates that the magnetic torque $\mu_{\perp} B$ imparts a large force to a cell attached to the magnetic posts. This force, F_{Mag}, can be obtained from the bending characteristics of

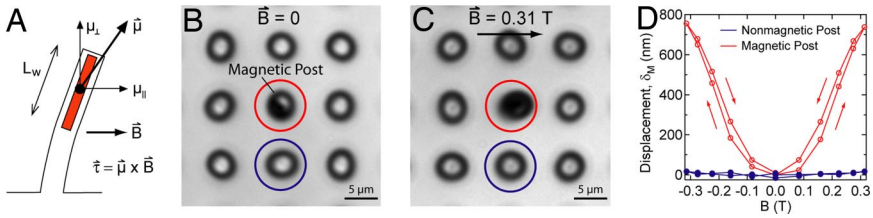

Fig. 2. Characterization of magnetic post actuation. (*A*) The magnetic torque, τ, on a magnetic post of length L depends on the applied field, $\vec{B}$, the nanowire length, L_W, and dipole moment, $\vec{\mu}$. (*B* and *C*) Phase-contrast micrographs of a magnetic post deflected under no field and a 0.31-T field. (*D*) Plots of post displacement versus applied field with arrows indicating direction of driving magnetic field. Actuations caused negligible mechanical displacement in adjacent nonmagnetic post (blue curve).

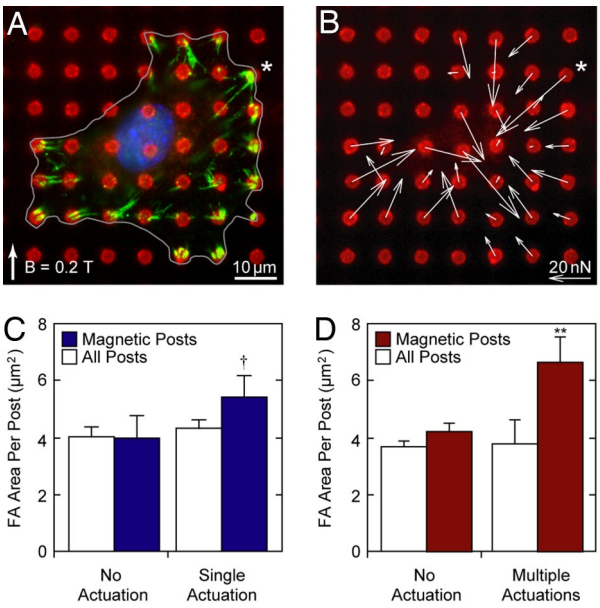

Fig. 3. FA protein recruits to site of external force application. (*A*) Representative immunofluorescent micrograph of FAs (green), microposts (red), and nucleus (blue) after force actuation. The direction and magnitude of the field are shown. The cell is outlined, and the location of the magnetic post is marked by the asterisk (*). (*B*) Vector plot of traction forces at each post are shown with white arrows. The cell is outlined, and the location of the magnetic post is marked by the asterisk (*). (*C*) Plot of average FA area for all posts underneath cells (white bars) and average FA area at magnetic posts (blue bars) when cells are subjected to no actuation and single actuation (†, $P = 0.0875$). (*D*) Plot of average FA area for cells subjected to no actuation and multiple actuations (**, $P = 0.0041$). (Error bars on all graphs denote standard error of the mean.)

a nanowire–PDMS composite post pinned at its free end by the cell, which we calculated by using Castigliano's first theorem for bending strain energy in a composite cantilever (27). The elasticity modulus along the beam is $E(x) = E_{\mathrm{PDMS}}$ for $0 \le x < L - L_W$ and $E(x) = E_{\mathrm{Co}}$ for $L - L_W \le x \le L$. Assuming that $E_{\mathrm{Co}} \gg E_{\mathrm{PDMS}}$, and solving for the reaction force at $x = L$, the force transmitted to the local FAs is

$$F_{\mathrm{Mag}} = \frac{3\mu_{\perp}B(L + L_w)}{2(L^2 + L_wL + L_w^2)}. \qquad [1]$$

For the magnetic post in Fig. 2, in which $L_W \approx 5$ μm and a torque $\mu_{\perp}B \approx 210$ nN·μm was applied at $B = 0.31$ T, this yields $F_{\mathrm{Mag}} \approx 27$ nN. Cells on nonmagnetic posts generate traction forces of 1–100 nN (10, 25), and thus these measurements indicate that magnetic posts can transmit external forces to a cell that are comparable to the cell's internally generated forces. Moreover, magnetic posts behave as simple springs and also can be used to measure traction forces.

FA Response to External Force. Using this system, we can measure changes in cells at their FAs and traction forces in response to external force (Fig. 3 *A* and *B*). We first examined whether external forces could elicit changes in FA size. We seeded NIH 3T3 cells onto arrays of posts, applied a constant 0.2-T horizontal field for 10 min to actuate the magnetic posts, fixed the cells immediately after stimulation, and immunostained for vinculin to quantify average FA area. For cells not exposed to a magnetic field, the average areas of FAs at magnetic posts were similar to those at nonmagnetic posts (Fig. 3*C*; 13 cells). However, for cells stimulated with a single force actuation, the average FA area was larger at magnetic posts than at nonmagnetic posts (Fig. 3*C*; 16 cells, $P = 0.0875$, paired Student's *t* test). These data suggest that FA growth is a localized effect to the FA experiencing force stimulation and does not affect the average FA size across the cell.

To control for direct effects of the magnetic field, cells on arrays of posts prepared without nanowires were subjected to a 0.2-T field for 10 min. Average FA areas were similar to those of unactuated controls, indicating that magnetic fields alone do not change FA area (data not shown). To confirm that changes in FA area were attributable to externally applied force, we used an alternative approach to mechanically displace nonmagnetic posts with a micromanipulator. Mechanical pulling on posts elicited a localized vinculin response similar to that obtained with magnetic actuation (SI Fig. 5).

The dynamics in force application also appears relevant for FA growth: we applied multiple actuations to cells within 10 min, with 2-min intervals with active field and 2-min intervals with no field. As before, average FA size was indistinguishable between magnetic and nonmagnetic posts in unstimulated controls (Fig. 3*D*; 12 cells). Interestingly, average FA area at actuated magnetic posts was significantly larger than average FA area for nonmagnetic posts (20 cells, $P = 0.0041$, paired Student's *t* test). These findings demonstrate that multiple stimulations increased FA size more than single actuations did. Together these single and multiple actuation studies support previous studies that showed that applied forces can increase FA assembly (13, 14) and validate the use of this system to study cellular mechanotransduction.

Traction Force Response to External Force. To examine traction force changes in response to force stimulation, individual cells were monitored with live microscopy. Eighteen individual cells were subjected to force stimulation, and eight cells served as unstimulated controls. Cells were observed for 10 min, and then a step force was applied by introducing a 0.2-T field (defined as time $t = 0$) and held for an additional 10 min. A cell from each group is shown in Fig. 4*A*, where fixing and immunostaining were performed after observation of traction force dynamics. The displacements of all posts in the field of view were analyzed, including posts attached to the cells (A_i and B_i) and posts not attached to cells (Bkg). These deflections and their corresponding traction forces for all posts under cell A (A_i) and a subset of posts of interest (B_1, B_2, and Bkg) are plotted to illustrate the data obtained for each cell (Fig. 4*B* and SI Movie 2). Before force stimulation, all posts for cell A, including the magnetic post, demonstrated small but steady changes in traction force dynamics, greater than the uncertainty (<0.64 nN) in our force measurements from image analysis. At time $t = 0$ a force $F_{\mathrm{Mag}} = 1.3$ nN was applied via the magnetic post. The post A_2 shows minimal deflection, indicating that the cell has applied a counterbalancing force of comparable magnitude. Interestingly, traction forces abruptly decreased with greater magnitude at several other posts (e.g., A_1 and A_3) and increased at others (e.g., A_6 and A_7). In comparison, no noticeable changes were observed for any posts underneath cell B upon field application (e.g., B_1 and B_2).

To describe and compare the mechanical response of stimulated and unstimulated cells, we calculated the average strain energy per post *u* caused by traction forces for each cell, as a physical measure of aggregate cellular contractility:

$$u = \frac{1}{N}\sum_i \frac{1}{2}k\delta_i^2, \qquad [2]$$

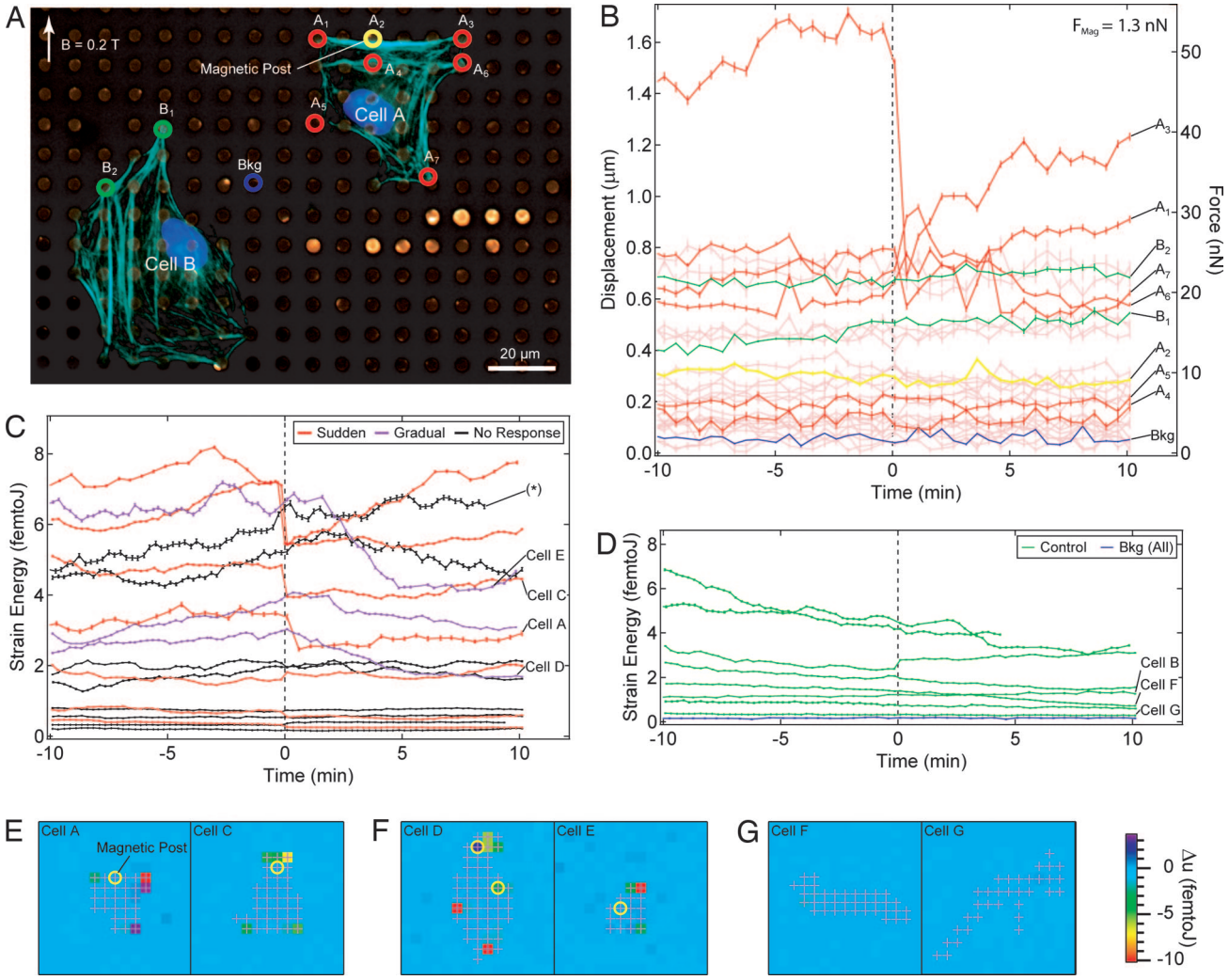

Fig. 4. Changes in traction forces in cells after force application. (*A*) Immunofluorescent micrograph of cell A, force-stimulated with a magnetic post, and cell B, unstimulated control. Labeling for actin (cyan), nuclei (blue), and PDMS (brown) were performed immediately after traction force video observation. Posts of interest are marked with colored circles and labeled according to which cell they were attached to (A_i or B_i) or background (Bkg). (*B*) Plot of displacement and force versus time for all posts for cell A (light red). A subset of posts of interest are designated (A_I, red; B_I, green; magnetic post A_2, yellow; and background post, blue). Onset of force stimulation is indicated by dashed line ($t = 0$). The force reported by the deflection also reflects cellular traction forces, except for A_2, which has an additional magnetic force component of 1.3 nN introduced at $t = 0$. (*C*) Plot of average strain energy per post (u) versus time for force-stimulated cells. Each cell is categorized by their response: sudden (red), gradual (purple), and no apparent (black) response. The cell marked with asterisk (*) has large strain energy and is shown with a scaling reduction of 3. (*D*) Plot of u versus time for unstimulated control cells (green) and background posts for all experiments (blue). (*B–D*) Error bars for all graphs indicate uncertainty in analysis. (*E*) Spatial plots of change in strain energy (Δu_i) in posts immediately before and after force application for stimulated cells that have sudden responses. Posts underneath each cell are shown in each plot (+). For each spatial plot, the direction of applied field ($B = 0.2$ T) is upward. For cell A, $F_{Mag} = 1.3$ nN, and for cell C, $F_{Mag} = 3.3$ nN. For posts with Δu_i outside the range of the scale, they are colored as the nearest extrema. (*F*) Spatial plots of Δu_i in posts immediately before and 10 min after for stimulated cells responding with gradual changes in energy. For cell D, $F_{Mag,\ top} = 5.4$ nN and $F_{Mag,\ bottom} = 6.2$ nN, and for cell E, $F_{Mag} = 3.9$ nN. (*G*) Spatial plots of control cells comparing Δu_i immediately before and after force application.

where δ is the displacement of the ith of N posts having spring constant k.[§] As expected from the observed changes in traction forces measured at some individual posts (e.g., A_1 and A_3), cell A displayed a loss of contractility (strain energy) when the field was applied, whereas cell B was unaffected (Fig. 4 *C* and *D*). Applying this measure of cellular contractility for all stimulated cells in the experiment, we observed a sudden loss in contractility upon force application in 33% (6 of 18) of cells, a gradual decrease in contractility over several minutes in 17% (3 of 18) of cells, and one cell exhibited a sudden increase in contractility. In contrast, control cells did not show any significant changes upon force stimulation, with the exception of one cell that showed an increase in contractility. We cannot exclude the possibility for this cell that application of the field inadvertently perturbed the culture mechanically, leading to the observed effect. To explore the basis for the three different responses in stimulated cells (sudden, gradual, or no change in contractility), we examined several parameters. Baseline levels of contractility before actuation in stimulated and control cells were similar in means and variances and did not correlate to response ($P > 0.1$, Student's t test and F test). We also did not observe a correlation between the location of force application (peripheral versus interior post) and the type of cellular response. Regardless, these data clearly

[§]The average strain energy u as calculated does not account for the applied force at the magnetic posts. An upper bound to the missing strain energy, provided by observed deflections in the absence of cells, contributes only an additional 0.04 fJ to u at $t = 0$.

demonstrate that even relatively small applied forces (total energy <1.5 fJ) can lead to massive adjustments in the internally generated cellular traction forces (total energy from 3–72 fJ).

One strength of this approach is that in addition to probing the global dynamic cellular force response to a perturbation, one also can examine the spatial distribution of the response. Here, one possibility is that the applied force is primarily affecting the response of nearby posts, whether through direct mechanical perturbation or through local propagation of biochemical signals. However, examining the data set for cell A (Fig. 4 *A* and *B*), it is clear that within the local vicinity of the applied force (e.g., A_4), traction forces did not significantly change after force application. In contrast, the subset of posts that exhibited a significant change in traction forces (e.g., A_1, A_3, A_6, and A_7) appeared to occur at the periphery of the cell. To explore this spatial effect further in the entire set of cells, we generated difference images indicating the change in strain energy over time for each post as a function of its position in the *X*–*Y* grid. For cells that experienced a sudden response in contractility upon force stimulation (Fig. 4*E*), these images (comparing immediately before and after force application) revealed that the change indeed occurred along a portion of the cell's perimeter, whereas posts in the interior of the cell showed no clear response to force stimulation. Cells experiencing gradual changes (comparing just before and 10 min after force application) similarly showed effects primarily at a few select posts along the perimeter (Fig. 4*F*). For both sudden and gradual responses, the change in strain energy per post $|\Delta u_i|$ is significantly higher for edge posts than for interior posts ($P < 0.05$). Further, upon grading posts with $\Delta u_i < -2$ fJ as responsive and the rest as unresponsive, a binomial analysis (28) shows that the probability of a post responding to the stimulus is significantly greater for an edge post than for an interior post ($P < 0.05$). Interestingly, posts that were nearest neighbors to the magnetic post did not show a preferential response over nonneighbor posts ($P > 0.25$). In contrast to stimulated cells, control cells exhibited little change in contractility, as shown in Fig. 4*G*, when compared immediately before and after the application of magnetic field. Thus, this spatial analysis suggests that the effects of external forces on cellular traction forces neither are localized around the site of force application nor do they lead to a homogeneous change in traction forces across the cell but instead appear to cause changes in the traction forces at the peripheral adhesions of a cell.

Discussion

Mechanical forces are pervasive within biological systems, whether originating in pathological or developmental settings. To characterize such forces, numerous methods have been developed to apply mechanical forces to cells or to measure cellular traction forces. Here, we have combined force application and measurement into a single device and used it to demonstrate an interplay between extracellular and intracellular forces that may be important in regulating cell function.

Incorporation of magnetic nanowires into a PDMS micropost device allowed us to apply nanonewton forces to individual FAs, as compared with the piconewton forces typically available with optical tweezers (18). Because of their high aspect ratio, nanowires retain high magnetic moments along their long axis in a nearly perpendicular magnetic field. In contrast, spherical magnetic particles of equal mass easily can reorient their internal magnetic moments, losing torque. Thus, this strategy allowed us to use a uniform magnetic field to apply essentially equal torque to all magnetic posts across a substrate, whereas magnetic spheres typically are manipulated individually by using a magnetic tweezer with a high gradient field (19).

Previous work has shown that applying a mechanical force to bound integrins will cause FA assembly (13, 14), but it has been unclear whether such a force would indirectly affect other FAs. Here, by applying force directly to a basal adhesion, we were able to compare forced and unforced FAs and to demonstrate that a locally applied force leads to FA assembly at the site of force application without causing global FA growth. We also found that multiple actuations yielded greater FA recruitment as compared with single actuations. Repeatedly applied forces also can lead to mechanical strengthening of adhesions (9, 10). These results indicate that there exist adaptive processes to regulate both FA size and strength. To further characterize these adaptive mechanisms, additional studies will be required; for example, there could be an optimal frequency, rate, or amplitude of force application to enhance the cellular response. Nonetheless, the local recruitment seen here implies that a cell may be able to use its many FAs to detect spatial variations in the stress field that arise in the underlying extracellular matrix.

Unexpectedly, externally applied force from magnetic posts caused a loss of traction forces at a subset of posts, mostly at the cellular periphery. Interestingly, the energy introduced to cells by the magnetic actuation (<1.5 fJ) was substantially less than the subsequent change in strain energy (3–72 fJ), highlighting the potential importance of traction forces in amplifying external mechanical signals. These changes in traction forces could be mediated by a biochemical event, such as activation or inactivation of a regulating signal, or by a mechanical event, such as fracturing of a cytoskeletal component. One possible pathway for such transmission involves calcium signaling, which has been shown to respond to mechanical stimulation and alter actomyosin dynamics (19, 29). However, the heterogeneous distribution of responsive versus nonresponsive microposts across the cells suggests that the existence of spatially directed signaling is not explained by simple diffusive mechanisms. The preexistence of a network of cytoskeletal filaments that is concentrated at discrete locations likely contributes to this spatially heterogeneous response (30, 31). External force could be transmitted directly across such a network to specific regions within the cells. Such global coordination of mechanical responses could be an important aspect of many processes, including cell spreading, polarization, division, and migration. Although the current study focused on a very short (10-min) window after stimulation in which motility was not a factor, it would be interesting to explore whether locally applied forces could affect the direction of migration and whether cells in different mechanical states (sessile versus migratory, spreading versus retracting) might respond to forces differently. Nonetheless, regardless of the mechanism, it appears that cells adapt to changes in their mechanical environment in part by relaxing their current mechanical state, remodeling, and reengaging the actomyosin cytoskeleton.

In summary, this study demonstrates the utility of the magnetic and nonmagnetic posts system for understanding how cells spatiotemporally control contractility in response to external forces. Traction forces responded quickly to externally applied forces or appeared to adapt thereafter with possible long-lasting effects on the tensional homeostasis of cells. These data highlight how adaptive mechanical changes within cells are potentially important in understanding how external forces are transduced into biochemical regulators of cell function and underscore the need for deeper insight into the interaction between external and internal forces.

Materials and Methods

Cell Culture and Reagents. NIH 3T3 mouse fibroblasts (ATCC CRL-1658) were cultured as described in ref. 10.

Fabrication and Characterization of Magnetic Nanowires. Nanowires were formed by electrochemical deposition in the pores of 50-μm-thick alumina filter templates (Whatman, Middlesex, U.K.) with nominal pore diameter of 350 nm. Cu was sputter-

coated onto one side of the template as the working electrode. Co was deposited from an aqueous solution of 0.5 M $CoSO_4$, 0.5 M NaCl, and 0.8 M H_3BO_4 (pH 3.3) at −1.0 V (Ag/AgCl) to form Co nanowires in the template pores, with lengths controlled by the total charge deposited. Cu was removed in a solution of 0.1 M $CuCl_2$ and 1 M HCl and the template was dissolved in deoxygenated KOH for 20 h with initial pH 12.8 and 4 h with initial pH 12.4. The nanowires in suspension were collected by using a permanent magnet and cleaned with ethanol. To characterize their magnetic properties, ~10^6 nanowires were oriented in a 0.2-T field, encased in 0.5 ml of epoxy (Araldite 502), and measured at room temperature with a vector vibrating sample magnetometer (DMS Model 10; ADE Technologies, Westwood, MA) (32).

Fabrication and Characterization of Magnetic Posts. Silicone micropost arrays were fabricated via replica-molding as described in ref. 10. Co nanowires were suspended in ethanol, distributed over the surface of PDMS (Sylgard 184; Dow-Corning, Midland, MI) micropost templates, and oriented vertically by placing NdFeB magnets underneath the templates. After the nanowires settled into the templates, the ethanol was evaporated at 70°C. Liquid PDMS prepolymer was poured over the template and cured at 110°C for 20 h, after which the post arrays were peeled from the templates. Selected magnetic posts were imaged in a SEM (6700F; JEOL, Tokyo, Japan) by using backscattering imaging and energy-dispersive x-ray microanalysis. The bending stiffness of the nonmagnetic and magnetic posts was measured with a pulled glass needle (World Precision Instruments, Sarasota, FL) mounted onto a micromanipulator (Cascade Microtech, Beaverton, OR). Video microscopy and computer-controlled electromagnets were used to characterize the actuation of selected magnetic posts. Before seeding cells, the locations of all of the magnetic posts were mapped by recording their deflections upon actuation with NdFeB magnets.

Culture of Cells on Micropost Arrays. Substrates containing the micropost arrays were prepared for cell attachment with fibronectin (50 μg/ml; BD Biosciences, San Jose, CA) as described in ref. 10. The arrays were fluorescently labeled with 5 μg/ml Δ^9-DiI (Invitrogen, Carlsbad, CA) and blocked from protein adsorption with 0.2% Pluronics F127 NF (BASF, Ludwigshafen, Germany). Cells were seeded onto arrays of posts, allowed to spread overnight, and then placed into a stage incubator (LiveCell; Pathology Devices, Westminster, MD) that was equipped with permanent magnets on a sliding rail mechanism to apply magnetic fields.

Quantification of FA Size. FA immunostaining and analysis was performed as previously described by using anti-vinculin antibody (hVin1; Sigma, St. Louis, MO) (6). Image analysis and quantification of FAs (identified as structures larger than 0.07 μm^2) were performed by using IPLab (BD Biosciences Bioimaging).

Quantification of Traction Forces. Traction forces were determined from fluorescent images of posts by using analysis software written in IgorPro (WaveMetrics, Lake Oswego, OR) and Matlab (Mathworks, Natick, MA). Intensity profiles for images of posts were modeled as two-dimensional Gaussian fits, and the position of each post was determined by a nonlinear least-squares fit to this model. The undeflected positions of posts under the cells were determined by using "empty" posts without cells on them around the border of each image as reference points for interpolation. Note that, with this approach, the net sum of forces on the cell is not preset to zero but falls below the expected error (1–2 nN per post). The posts' displacement vectors were converted to force maps by using the measured average post spring constant $k = 32$ nN/μm as described in ref. 10.

Spatial Maps. Changes in strain energy were calculated from the difference in the time-averaged intervals before application of the field ($t = -1.25$ to -0.25 min) and afterward ($t = 0$ to 1 min or $t = 9$ to 10 min). The statistical significance of the regional comparisons were calculated by using a one-tailed Wilcoxon rank-sum test on the average of the absolute change in strain energy per post and a binomial test for responsive posts ($\Delta u_i < -2$ fJ) as described in ref. 28.

We thank J. Tan, D. Cohen, R. Desai, S. Raghavan, and K. Bhadriraju for helpful discussions and ideas. This work was supported in part by grants from National Heart, Lung, and Blood Institute, National Institute of Biomedical Imaging and Bioengineering, Army Research Office Multidisciplinary University Research Initiative, the Material Research Science and Engineering Center of The Johns Hopkins University, and the Nano/Bio Interface Center of the University of Pennsylvania. N.J.S. acknowledges financial support by the Hartwell Foundation and the National Institutes of Health's National Research Service Award.

1. Chen CS, Tan J, Tien J (2004) *Annu Rev Biomed Eng* 6:275–302.
2. Davies PF, Barbee KA, Volin MV, Robotewskyj A, Chen J, Joseph L, Griem ML, Wernick MN, Jacobs E, Polacek DC, *et al*. (1997) *Annu Rev Physiol* 59:527–549.
3. Katsumi A, Milanini J, Kiosses WB, del Pozo MA, Kaunas R, Chien S, Hahn KM, Schwartz MA (2002) *J Cell Biol* 158:153–164.
4. Sawada Y, Sheetz MP (2002) *J Cell Biol* 156:609–615.
5. McBeath R, Pirone DM, Nelson CM, Bhadriraju K, Chen CS (2004) *Dev Cell* 6:483–495.
6. Pirone DM, Liu WF, Ruiz SA, Gao L, Raghavan S, Lemmon CA, Romer LH, Chen CS (2006) *J Cell Biol* 174:277–288.
7. Geiger B, Bershadsky A, Pankov R, Yamada KM (2001) *Nat Rev Mol Cell Biol* 2:793–805.
8. Vogel V, Sheetz M (2006) *Nat Rev Mol Cell Biol* 7:265–275.
9. Balaban NQ, Schwarz US, Riveline D, Goichberg P, Tzur G, Sabanay I, Mahalu D, Safran S, Bershadsky A, Addadi L, Geiger B (2001) *Nat Cell Biol* 3:466–472.
10. Tan JL, Tien J, Pirone DM, Gray DS, Bhadriraju K, Chen CS (2003) *Proc Natl Acad Sci USA* 100:1484–1489.
11. Burridge K, Chrzanowska-Wodnicka M (1996) *Annu Rev Cell Dev Biol* 12:463–518.
12. Bershadsky A, Kozlov M, Geiger B (2006) *Curr Opin Cell Biol* 18:472–481.
13. Riveline D, Zamir E, Balaban NQ, Schwarz US, Ishizaki T, Narumiya S, Kam Z, Geiger B, Bershadsky AD (2001) *J Cell Biol* 153:1175–1186.
14. Galbraith CG, Yamada KM, Sheetz MP (2002) *J Cell Biol* 159:695–705.
15. Giannone G, Sheetz MP (2006) *Trends Cell Biol* 16:213–223.
16. Geiger B (2006) *Cell* 127:879–881.
17. Wang N, Butler JP, Ingber DE (1993) *Science* 260:1124–1127.
18. Choquet D, Felsenfeld DP, Sheetz MP (1997) *Cell* 88:39–48.
19. Matthews BD, Overby DR, Mannix R, Ingber DE (2006) *J Cell Sci* 119:508–518.
20. Shirinsky VP, Antonov AS, Birukov KG, Sobolevsky AV, Romanov YA, Kabaeva NV, Antonova GN, Smirnov VN (1989) *J Cell Biol* 109:331–339.
21. Shiu YT, Li S, Marganski WA, Usami S, Schwartz MA, Wang YL, Dembo M, Chien S (2004) *Biophys J* 86:2558–2565.
22. Beningo KA, Wang Y-L (2002) *Trends Cell Biol* 12:79–84.
23. Bao G, Suresh S (2003) *Nat Mater* 2:715–725.
24. Sniadecki NJ, Desai RA, Ruiz SA, Chen CS (2006) *Ann Biomed Eng* 34:59–74.
25. Lemmon CA, Sniadecki NJ, Ruiz SA, Tan JL, Romer LH, Chen CS (2005) *Mech Chem Biosyst* 2:1–16.
26. Landau LD, Lifshitz EM, Pitaevskii LP (1984) *Electrodynamics of Continuous Media* (Pergamon, Oxford, UK).
27. Boresi AP, Sidebottom OM (1985) *Advanced Mechanics of Materials* (Wiley, New York).
28. Schmidt CE, Horwitz AF, Lauffenburger DA, Sheetz MP (1993) *J Cell Biol* 123:977–991.
29. Cristofanilli M, Akopian A (2006) *J Physiol* 575:543–554.
30. Ingber DE (2003) *J Cell Sci* 116:1397–1408.
31. Blumenfeld R (2006) *Biophys J* 91:1970–1983.
32. Hultgren A, Tanase M, Chen CS, Meyer GJ, Reich DH (2003) *J Appl Phys* 93:7554–7556.